Tonic resting-state hubness supports high-frequency activity defined verbal-memory encoding network in epilepsy

Running Title IEEG-HFA integrated memory hubness in epilepsy

Author Affiliations:

Chaitanya Ganne[1], Walter Hinds[2], James Kragel[3], Xiaosong He[1], Noah Sideman[1], Youssef Ezzyat[3], Michael R Sperling[1], Ashwini Sharan[4], and Joseph I Tracy[1]*

[1]Department of Neurology, Thomas Jefferson University, Philadelphia, Pennsylvania, 19107

[2]School of Biomedical Engineering, Science and Health Systems, Drexel University, Philadelphia, Pennsylvania, 19104

[3]Department of Psychology, University of Pennsylvania, Philadelphia, Pennsylvania, 19104

[4]Department of Neurosurgery, Thomas Jefferson University, Philadelphia, Pennsylvania, 19107

* **Corresponding Author** Joseph I. Tracy, Ph.D.

Professor, Departments of Neurology and Radiology

Director, Clinical Brain Mapping and Cognitive Neuroscience Laboratory

Thomas Jefferson University, Sidney Kimmel Medical College

901 Walnut Street, Suite 447

Philadelphia, PA, 19107

Phone: (215)955-4661

Fax: (215)955-3745

Email: Joseph.Tracy@Jefferson.edu

Number of text pages (Introduction, Methods, Results, Discussion): 27

Number of words in the abstract: 151

Number of words: 7252

Number of references: 62

Number of figures: 6

Number of tables: 3

Numbers of Supplementary materials: 1 (1 text file inclusive of figure and tables)

Abstract

High-frequency gamma activity (HFA: 45–95Hz) on invasive-electroencephalogram coupled with verbal-memory encoding has laid the foundation for numerous studies testing the integrity of memory in diseased populations. Yet, the functional connectivity characteristics of networks subserving these HFA-memory linkages remains uncertain. By integrating this electrophysiological biomarker of memory encoding from IEEG with resting-state BOLD fluctuations, we estimated the segregation and hubness of HFA-memory regions in drug-resistant epilepsy patients and matched healthy controls. HFA-memory regions express distinctly different hubness compared to neighboring regions in health and in epilepsy, and this hubness was more valuable than segregation in predicting verbal memory encoding. The HFA-memory network comprised regions from both the cognitive control and sensorimotor processing networks, validating that effective verbal-memory encoding requires multiple functions, and is not dominated by a central cognitive core. Our results demonstrate a tonic intrinsic set of functional connectivity, which provides the necessary conditions for effective, phasic, task-dependent memory encoding.

Key Words Verbal memory, High-frequency activity, Betweenness centrality, Hubness, Participation coefficient, Random forest

Abbreviations

HFA – High frequency activity

MEM - Brain regions showing HFA associated with verbal-memory encoding

CN - Controls Nodes

P.REC - Percentage of words recalled during IEEG memory testing

CVLT - California Verbal Learning Test

Highlights

1. High gamma memory activity in IEEG corresponds to specific BOLD changes in resting-state data.
2. HFA-defined memory regions had lower betweenness centrality relative to neighbouring control nodes in both epilepsy patients and healthy controls.
3. The betweenness centrality hubness of the HFA-memory network was distinct from other cognitive networks.
4. HFA-memory network shares regional membership and interacts with multiple cognitive networks required for successful verbal memory encoding.
5. HFA-memory network hubness predicted both concurrent task (phasic) and baseline (tonic) verbal-memory encoding success.

Introduction

Human high-frequency activity (HFA: 45–95Hz) captured using invasive electroencephalography (IEEG) is associated with neuronal firing during episodic memory encoding, termed the 'Subsequent Memory Effect' (SME)(Burke JF et al., 2015;Greenberg JA et al., 2015;Jensen O et al., 2007). The majority of this work has been done in patients undergoing IEEG implantation for drug-resistant epilepsy (DRE)(Burke JF, et al., 2015;Greenberg JA, et al., 2015;Lega B et al., 2014;Long NM et al., 2014;Solomon EA et al., 2017). This link between HFA and verbal-memory encoding has been validated using both power-amplitude analysis and phase synchronization (Burke JF, et al., 2015;Burke JF et al., 2013;Greenberg JA, et al., 2015;Lega B, et al., 2014;Long NM, et al., 2014). Despite these well-established linkages, little is known about the network organization and the degree to which these HFA regions either possess distinct network features relative to other brain regions or rely on abnormal organizational properties due to epilepsy. The impact of seizures on the brain is known to go beyond the epileptogenic zone (Burns SP et al., 2014;Fahoum F et al., 2012;Tracy JI et al., 2015). While evidence exists to suggest that memory-relevant regions in the epileptic brain can take up normative network roles in an effort to preserve function (Jin SH et al., 2015;Powell HW et al., 2007;Solomon EA, et al., 2017;Tracy J et al., 2014), the network properties characterizing these memory regions in health and in disease are unclear. In this study, we integrate IEEG with resting-state fMRI (rsfMRI) data to characterize the network architecture of a task-defined HFA-memory network and understand its relationship to the functional connectivity of a broader set of intrinsic resting-state networks. Graph theory has been a useful tool for mapping functional networks and characterizing their properties during task and at rest. Two important graph indices that are essential in characterizing brain regions and their functionality include: (1) clustering coefficient, which captures network segregation and local

information processing and (2) betweenness centrality, which captures hubness and the degree of importance held by a region that connects two or more modules (Power JD et al., 2013). Through network neuroscience measures of hubness and segregation, we define and broaden our understanding of the network characteristics that support memory encoding, and reveal the contribution of multiple intrinsic networks to successful memory encoding.

Prior studies combining IEEG and fMRI have shown a good correspondence between HFA and blood oxygen level dependent (BOLD) contrast signal, offering a key link between electrophysiological and hemodynamic properties of human memory (Axmacher N et al., 2008;Jacques C et al., 2016;Khursheed F et al., 2011;Logothetis NK et al., 2001;Rugg MD et al., 2002). Integrating IEEG with rsfMRI has the advantage of sampling the wider brain regions, allowing us to test the correspondence between the information embedded in the faster dynamics of IEEG data (i.e., HFA) and the slower BOLD response (Esposito F et al., 2013;Mizuhara H, 2012;Mizuhara H et al., 2005;Murta T et al., 2017). In this study, we address four specific questions: First, how does the resting-state functional connectivity (rsFC) of the HFA-memory network involved in verbal-memory encoding differ from neighboring regions that lack significant SME? Second, are the network characteristics of HFA-memory regions in epilepsy patients generalizable, or, do they differ from those of matched healthy controls? Third, by discovering the key features of the HFA-memory network and studying their relationship to other intrinsic networks, can we reveal the trait-like properties of the intrinsic state, as well as the constituent cognitive processes that are necessary for effective memory encoding? Fourth, are HFA-memory network characteristics associated with and able to predict clinically relevant verbal-memory performance in epilepsy?

2 METHODS

2.1 Participants

Thirty-seven patients with DRE were recruited from the Thomas Jefferson University (TJU) Comprehensive Epilepsy Center. They underwent IEEG implantation (subdural, depth, or both) to localize the epileptogenic zone and guide potential surgical management of their seizures (Figure 1) (Table 1). Site and reason for implantation were determined by multimodal pre-surgical evaluation including neurological history and examination, video-EEG, MRI, PET, and neuropsychological testing (Sperling MR et al., 1996). Specific to this study, patients underwent a 3T-MRI scan (rsfMRI+T1MPRAGE) (Philips Achieva, Amsterdam, Netherlands), pre-surgical neuropsychological assessment (NPA) to provide a baseline indication of the patients verbal-memory skills, followed by IEEG implantation and monitoring (Nihon Kohden EEG-1200, Irvine, CA) during which patients participated in verbal episodic memory testing (free-recall paradigm). This provided behavioral measures at two stages of clinical evaluation: percent recall from a word-list memory test administered simultaneously with IEEG recording (P.REC) and the sum-total of words recalled from a similar memory test administered during baseline neuropsychological testing (CVLT Total Learning - CVLT-TL) (Supplementary Methods, Data Acquisition).

Patients were excluded from the study for any of the following reasons: previous brain surgery; medical illness with central nervous system impact other than epilepsy; contraindications to MRI; or hospitalization for any Axis I disorder listed in the Diagnostic and Statistical Manual of Mental Disorders, IV. Depressive disorders were allowed given the high comorbidity of depression and epilepsy (Tracy et al., 2007). Healthy controls (HC, N=37) were recruited to match the patients in age, gender, handedness, and education. All participants provided written informed consent as per the TJU Institutional Review Board requirements.

2.2 IEEG acquisition and free-recall testing

IEEG data were recorded from neurosurgical patients performing delayed free recall of categorized and unrelated word lists. The task was presented at the bedside using PyEPL software and the IEEG data was simultaneously recorded using the Nihon-Kohden IEEG system [sampling rate >500Hz] (Geller AS et al., 2007). Participants were instructed to commit each list of words to memory. Recalled responses were digitally recorded and parsed/scored offline using the University of Pennsylvania Total Recall program (http://memory.psych.upenn.edu/TotalRecall) (Supplementary figure 1). Participants performed up to 25 recall trials in a single recall session (Supplementary Methods).

HFA power was compared between words that were subsequently remembered or forgotten (through retrospective binning of responses), providing a measure of the subsequent memory effect (SME) at each bipolar pair. HFA power was calculated on logarithmically spaced wavelets ranging from 44–100 Hz, on a notch filtered (58-62Hz) data (Supplementary Methods, Data Analysis for details). For every bipolar pair and encoding period (1600ms/word), the difference in spectral power during memory formation was calculated by computing t-statistic, comparing the distributions of event-averaged power values associated with all successful and unsuccessful encoding trials.

Subsequently, anatomic localization of bipolar pairs (computed as the mid-point between the two contacts) was accomplished using 2 independent processing pipelines for depth and surface electrodes which were later transformed to MNI space similar to previous studies (Burke JF, et al., 2013;Kragel JE et al., 2017).

2.3 Functional MRI data acquisition and preprocessing

All participants (patients and healthy controls) underwent a rsfMRI scan using single shot echo planar gradient echo sequence (120 volumes; 34 slices; TR = 2.5s, TE = 35ms; flip angle (FA) = 90°, FOV=256 mm, 128×128 matrix, resolution: 2×2×4mm) in a 3T MRI scanner (Philips Achieva). T1-MPRAGE images (180 slices, 256×256 isotropic 1mm voxels; TR/TE/FA=640ms/3.2ms/8°, FOV=256 mm) were also collected. Patients were instructed to stay awake, keep their eyes closed, and stay relaxed. All imaging data were preprocessed using Data Processing Assistant for rsfMRI Advanced Edition (http://www.rfmri.org/DPARSF)(Yan CG et al., 2010), a MATLAB toolbox based on Statistical Parametric Mapping-8 (http://www.fil.ion.ucl.ac.uk/spm/software/spm8) using the standard pipeline for rsFC (Supplementary Methods).

2.4 Graph Theory analysis

Using the Lausanne's 234 ROI atlas, 234 by 234 correlation-matrices were calculated at individual subject level, which were used subsequently to construct weighted undirected graphs. Minimal Spanning Tree (MST) based networks were derived to ensure the same number of connected nodes for all subjects, allowing for reliable group-level comparisons and yielding a series of graphs with connection density ranging from 5% to 50% in increments of 1% (van Diessen E et al., 2013) (Supplementary Methods). The density range of 5% to 50% was chosen for the following reasons: (1) network measures are relatively constant over this range (Alexander-Bloch AF et al., 2010); (2) previous work has suggested that above a density of 50% graphs become more random (Humphries MD et al., 2006) and prone to non-biological features and noise (Kaiser M et al., 2006). Using these graphs, clustering coefficient (CC) and betweenness centrality

(BC) were calculated using Brain Connectivity Toolbox (www.brain-connectivity-toolbox.net) (Rubinov M et al., 2010).

2.5 Defining HFA-memory regions (MEM) and their neighboring control nodes (CNs) for rsfMRI analysis

Brain regions where IEEG showed significant SME with increased HFA were termed HFA-memory regions (MEM). Brain regions where IEEG recorded HFA, but the results did not survive statistical significance for successful memory encoding were termed Control Nodes (CNs).

The 3731 IEEG bipolar contacts for all the patients were superimposed into a single MNI coordinate space, referred to as the “super-brain” (Figure 1, Supplementary figure 2 and 5).

Figure 1: Network construction and statistical analysis

This study pipeline illustrates the multi-staged approach in the study. Only patients underwent IEEG implantation, whereas the rsfMRI was acquired in both the patients and in healthy controls. The IEEG electrodes pooled from all the subjects were used to create a 'super-brain' to test the net memory encoding effect in the high gamma frequency (high frequency activity: HFA). For every HFA-memory region, three sets of neighboring controls nodes (CNs) were determined based on their Euclidean Distances (CN.1: first closest ED, CN.2: second closest ED and CN.RAND: a single random ED among the first 5 closest EDs). For all the 103 regions (MEM+CNs) together, we tested which of the graph measures, clustering coefficient (CC) or betweenness centrality (BC) were significantly different between MEM and CNs using a mixed-model ANOVA. We then tested the association of these graph measures with clinical memory performance (CVLT-TL and P.REC) using the random forest model.

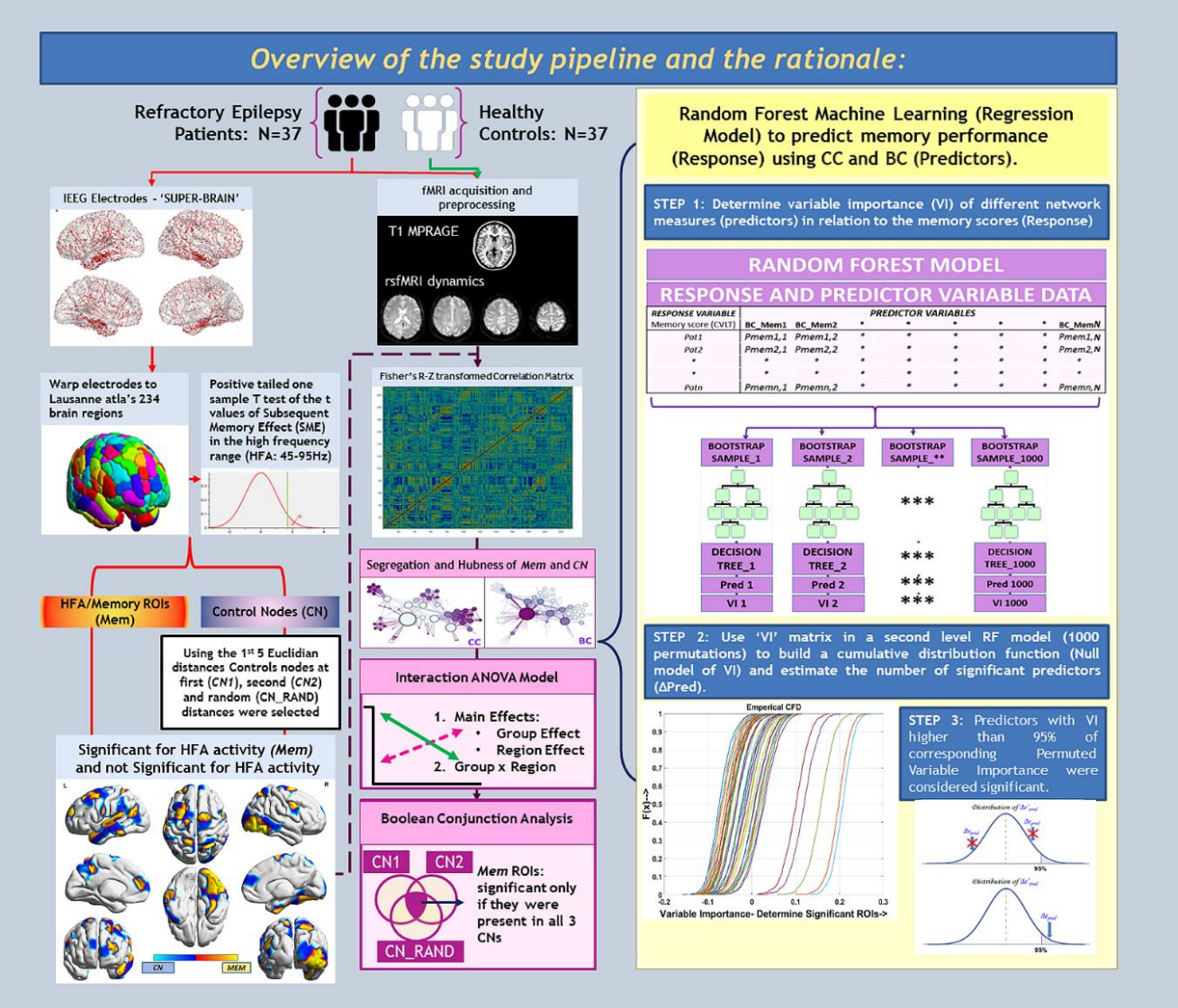

The MNI coordinates of these contacts were then warped to the nearest 3D Cartesian coordinates in the Euclidean space of each of the ROIs of the Lausanne atlas (Hagmann P et al., 2008). In order to avoid the probability of the algorithm wrongly assigning the electrodes to subcortical structures, we excluded these regions, yielding an atlas with 222 implant-relevant regions. Each electrode coordinate was warped to the coordinate of the nearest ROI of the Lausanne atlas (Supplementary Methods, Supplementary Figures 2 and 5). This allowed us to group the 3731

contacts into their respective 222 ROIs. Once this was done, the t-values of the multiple electrodes within each ROI were submitted to a positive tailed one-sample t-test to determine if there was a significant increase in HFA power between words that were encoded and words that were forgotten. To account for multiple comparisons, the P-values generated for the 222 ROIs were subjected to FDR correction (Genovese CR et al., 2002). The FDR corrected significant ROIs were considered to exhibit memory-relevant encoding effects, henceforth referred to as MEM ROIs.

For every MEM, we identified the nearest 5 CNs based on their Euclidian distance (ED), as these neighboring CNs had the highest chance of being implanted and providing contrasting HFA recordings. The ROIs closest to MEM were grouped as first control nodes (CN.1) and second closest as CN.2. To avoid bias of the distance from the MEM, we chose a random ROI among the first 5 EDs, and refer to these as the 'random distance control nodes' (CN.RAND) (Supplementary Methods, Figure 2, Supplementary Figure 3).

2.6 Hubness and Participation coefficient of the HFA-memory network in comparison with the intrinsic networks

Since the HFA-memory network was found to have regions distributed widely over the brain, we were interested in looking at whether the HFA-memory regions had membership in other intrinsic networks. Hence, we assigned the different regions of the Lausanne's atlas to the different intrinsic networks as defined by Gu et al (Gu S et al., 2015). Along with BC, we also estimated the participation coefficient (PC) using BCT (https://sites.google.com/site/bctnet/). While BC indicates regions that have considerable influence within a network by virtue of their control over information passing between others, it does not reveal anything about the diversity of inter-network connections of individual nodes. In contrast, PC helps identify influential nodes in a network that are likely to be

highly connected to other networks and, as a result, communicate and exert influence over these other networks.

2.7 Statistical analysis

Chi-square or t-tests, as appropriate, were used to compare the groups on demographic and clinical variables ($p<0.05$ was considered significant). To assess group (patient vs controls), region (MEM vs CN), and group-by-region effects, we ran a two-way ANOVA on the graph indices (CC and BC) at two levels: 1) the 'composite network' level and 2) 'individual region' level. At a 'composite network' level, the average-CC (AvgCC) and average-BC (AvgBC) across the separate MEM and CNs were calculated and served as the primary dependent variables in the ANOVAs. The ANOVAs contrasting the MEM with the three available CN ROI's (CN.1, CN.2, and CN.RAND) were run in separate models. At the 'individual region' level, the NodalCC and NodalBC of MEM and CNs served as the primary dependent variables in the ANOVAs. A MEM was considered significantly different from the CNs only when each MEM was shown to be reliably different from all three CNs (CN.1, CN.2, and CN.RAND) using Boolean conjunction analysis (Supplementary figure 4) (Figure 1) (Supplementary Methods). This method ensured that MEM ROIs with a significant difference in graph indices to only a single CN were not considered valid. Throughout the analysis, multiple comparison correction was calculated using the false discovery rate (pFDR) (Figure 1). The difference in AvgBC and AvgPC of the HFA-memory network in comparison with the intrinsic networks was tested using repeated measures ANOVA with Fisher's Least Significant Difference (LSD).

2.8 Multivariate machine learning to predict free-recall performance

We used a 'Random Forest' (RF) model to determine the relationship between fMRI graph indices (NodalBC and NodalCC, i.e., the predictor variables) and free-recall performance (P.REC and CVLT-TL, tested separately, i.e., the response variable). CVLT-TL is sensitive to memory encoding and immediate recall, comparable in this sense to the P.REC measure. (Table 1). RF is an efficient, supervised machine learning method that identifies both linear and non-linear brain-behavior relationships, allows simultaneous testing of multivariate interactions, and shows superior resilience to overfitting (Breiman L, 2001). The algorithm exploits random decision trees, which use a subset of the observations through bootstrapping techniques. In short, from the original data set a random selection of the training data is sampled and used to build a model. The model is then tested on the data not included in the training sample, referred to as "out-of-bag". Every time a model was built and applied to its "out-of-bag" data, the importance of each variable (VI) was estimated based on the increase of prediction error when "out-of-bag" data for that variable was permuted, while all others were left unchanged (Liaw A et al., 2002).

We first ranked the predictors using variable importance (VI) to identify the most relevant network properties using a permutation-based method (Altmann A et al., 2010). Briefly, we estimated the true VI for each predictor for 1000 repetitions. Next, we established a null distribution of VIs for every predictor by estimating their VI from models trained with the response variable randomly permuted a 1000 times. Based on the true VI, the VI of each predictor from each random permutation, a probability can be estimated based on its corresponding normal cumulative null distribution, with a variable considered significant if the probability is larger than 95%. Lastly, we selected predictors whose VIs were found significant at least 950 times over the 1000 repetitions, to build RF models and predict the response. The association between the

predictions and actual scores was tested using a right-tailed Pearson correlation. In addition, stepwise linear regression models (SRM) on the two response variables were run with the selected predictors from the RF models serving as independent variables, allowing us to explore any directional or ranking effects among the predictors (details in Supplementary Methods, Data Analysis).

3 RESULTS

3.1 Demographic and clinical characteristics of the groups (patients and controls)

The demographic details of the patients and healthy controls are listed in Table 1 (also Supplementary Table 1). They were matched for age, gender, handedness, years of education, and head micro-movement during rsfMRI ($p>0.05$). Relative to same age peers, the DRE patients had CVLT-TL performance in the average range (t=48, age-normed), indicating intact memory encoding ability.

Table 1: Demographic and clinical characteristics

Both DRE patients and healthy controls were matched for age, gender, handedness, education. After estimating the head motion we noticed that the values were low, as well as comparable, between the two groups. Further demographic data specific to the DRE patients have been enumerated in this table.

Sample Group (N)		**Patients** 37	**Controls** 37	**F/T/χ^2**	**P**
Age (M±SD)		36.86±10.69	33.91±12.65	1.08	0.28
Gender (M/F)		21/16	24/13	0.23	0.63
Education (years, M±SD)		13.67±2.62	14.2±1.72	-1.39	0.16
Handedness (R:L)		30/7	26/11	0.66	0.41
Head Motion (FD_Jenkinson)		0.12±0.01	0.10±0.04	-0.90	0.36

Free-recall Measures					
P.REC		21.15±9.2%			
CVLT-TL		48.4±11.2%			
Age at Epilepsy Onset (M±SD; years)		20.94±13.19	-	-	-
Duration of Epilepsy (M±SD; years)		15.92±10.25	-	-	-
Seizure Type			-	-	-
FOIA		6	-	-	-
FOIA+BTCS		17	-	-	-
FOIA/FOA		4	-	-	-
FOIA/FOA+BTCS		6	-	-	-
FOA+BTCS		4	-	-	-
Anti-Epileptic Drugs			-	-	-
VGNC	CBZ,OXC,LTG, PHT	24	-	-	-
GABAa Agonist	PB, BZD, Pr	7	-	-	-
SV2a Receptor Mediated	LVA	15	-	-	-
CRMP2 Receptor Mediated	LCM	8	-	-	-
Multi-Action	VPA, TPM, ZNS	17	-	-	-
VGCC	PGB, GBP	4	-	-	-

M: Mean, SD: Standard Deviation, FOA: Focal Onset Aware Seizures, FOIA: Focal Onset seizures with Impaired Awareness; BTCS: focal seizures progressing to bilateral tonic-clonic seizures, VGNC: Voltage-gated sodium channel blockers: CBZ: carbamazepine, OXC: oxcarbazepine, PHY: phenytoin, GABAa Agonist: Gamma amino butyric acid a receptor agonist: PB: barbiturates; BZDs: benzodiazepines (diazepam, lorazepam, clonazepam, clobazam); SV2a Receptor-Mediated AEDs: LVA: levetiracetam; CRMP2 Receptor-Mediated AEDs: LCM: lacosamide; VGCC: Voltage-gated calcium channel: PGB: pregabalin; GBP: gabapentin; Multi-action AEDs: VPA: valproate; TPM: topiramate; Pr: Primidone

3.2 Defining HFA-memory regions and their neighboring control nodes

Brain regions where IEEG showed significant SME with increased HFA were termed HFA-memory regions (MEM) (Figure 1). MEM regions included the ventral stream (lateral occipital regions and the inferotemporal surface consisting of the fusiform gyri, n.b., areas necessary for visual recognition), and through their connections with the medial temporal lobe formed a circuit supporting memory consolidation. MEM areas also included discrete regions of bilateral lateral neocortices involving the left rostral middle frontal, inferior temporal, cingulate, postcentral, inferior parietal, insular (LrMFG, LITG, LPostCinG, LIstCinG, LIPL, LInsG), bilateral superior frontal, parietal, inferior temporal, and fusiform gyri (B/LSFG, B/LSPG, B/LITG, B/LFusG) (pFDR<0.0058). The corresponding control regions (CNs – CN.1, CN.2, and CN.Rand) were identified based on the Euclidean distance proximity of neighboring ROIs to MEM ROIs (Table 2 and Figure 2).

Table 2: The IEEG derived HFA-memory regions (MEM) mapped to the Lausanne atlas brain ROIs and the corresponding control nodes (CN.1, CN.2, and CN.RAND)
The 3731 electrodes after being assigned to the different brain regions were tested for significant subsequent memory effect (MEM). Once these regions were derived based on nearest Euclidean distances we determined the three neighboring control nodes (CN.1, CN.2, and CN.RAND).

ROI#	**MEM**	ROI#	**CN.1**	ROI#	**CN.2**	ROI#	**CN.RAND**
26	RSFG.7	32	RPreCG.2	25	RSFG.6	38	RParaCG.2
33	RPreCG.3	36	RPreCG.6	27	RSFG.8	47	RPostCG.3
57	RSPG.4	56	RSPG.3	29	RcMFG.2	55	RSPG.2
78	RLatOG.3	76	RLatOG.1	44	RIstCinG.1	65	RIPG.5
79	RLatOG.4	77	RLatOG.2	58	RSPG.5	74	RPeriCaL1
80	RLatOG.5	83	RLinG.3	65	RIPG.5	77	RLatOG.2

84	RFusG.1	86	RFusG.3	66	RIPG.6	81	RLinG.1
85	RFusG.2	89	REntRG.1	81	RLinG.1	93	RITG.3
87	RFusG.4	95	RMTG.1	82	RLinG.2	94	RITG.4
94	RITG.4	96	RMTG.2	88	RPHG.1	115	RAmy
120	LparsOrb.1	117	LLatOrbFG.2	93	RITG.3	116	LLatOrbFG.1
124	LparsTri.1	119	LLatOrbFG.4	97	RMTG.3	129	LrMFG.3
128	LrMFG.2	127	LrMFG.1	118	LLatOrbFG.3	134	LSFG.2
130	LrMFG.4	129	LrMFG.3	125	LparsOp1	135	LSFG.3
132	LrMFG.6	133	LSFG.1	126	LparsOp2	136	LSFG.4
138	LSFG.6	141	LSFG.9	131	LrMFG.5	139	LSFG.7
140	LSFG.8	142	LcMFG.1	135	LSFG.3	142	LcMFG.1
158	LPostCinG.2	157	LPostCinG.1	137	LSFG.5	157	LPostCinG.1
159	LIstCinG.1	165	LPostCG.6	144	LcMFG.3	177	LSPG.6
166	LPostCG.7	180	LIPG.2	152	LPreCG.8	182	LIPG.4
174	LSPG.3	183	LIPG.5	154	LParaCG.2	188	LPC.5
179	LIPG.1	186	LPC.3	170	LSMG.4	201	LFusG.2
203	LFusG.4	201	LFusG.2	173	LSPG.2	217	LSTG.1
209	LITG.3	205	LEntRG.1	194	LLatOG.4	218	LSTG.2
210	LITG.4	212	LMTG.2	200	LFusG.1	220	LSTG.4
211	LMTG.1	217	LSTG.1	204	LPHG.1	221	LSTG.5
213	LMTG.3	219	LSTG.3	208	LITG.2	222	LTransTG.1
223	LIns.1	222	LTransTG.1	220	LSTG.4	231	LAccu
226	LIns.4	225	LIns.3	224	LIns.2	233	LAmy

ROI# - The ROI numbering as per the atlas; MEM – IEEG defined ROIs which were significant for HFA-memory activity; CN – Control nodes that are measured at 3 different Euclidean Distances; R.superiorfrontal (RSFG), R.precentral (RPreCG), R.superiorparietal (RSPG), R.lateraloccipital (RLatOG), R.fusiform (RFusG), R.inferiortemporal (RITG), L.parsopercularis (LparsOp), L.parstriangularis (LparsTri), L.rostralmiddlefrontal (LrMFG), L.superiorfrontal (LSFG), L.posteriorcingulate (LPostCinG), L.isthmuscingulate (LIstCinG), L.postcentral (LPostCG), L.superiorparietal (LSPG), L.inferiorparietal (LIPG), L.fusiform

(LFusG), L.inferiortemporal (LITG), L.middletemporal (LMTG), L.insula (LIns), R.lingual (RLinG), R.entorhinal (REntRG), R.middletemporal (RMTG), L.lateralorbitofrontal (LLatOrbFG), L.caudalmiddlefrontal (LcMFG), L.precuneus (LPC), L.entorhinal (LEntRG), L.superiortemporal (LSTG), L.transversetemporal (LTransTG), R.caudalmiddlefrontal (RcMFG), R.isthmuscingulate (RIstCinG), R.inferiorparietal (RIPG), R.parahippocampal (RPHG), L.precentral (LPreCG), L.paracentral (LParaCG), L.supramarginal (LSMG), L.lateraloccipital (LLatOG), L.parahippocampal (LPHG), R.paracentral (RParaCG), R.postcentral (RPostCG), R.pericalcarine (RPeriCaL), R.amygdala (RAmy), L.accumbensarea (LAccu), L.amygdala (LAmy)

Figure 2: HFA-memory regions (MEM) and their corresponding Control Nodes (CNs)

The warm yellow color represents the MEM ROIs (MEM) and the cool cyan color represents the controls nodes (CNs) which are the first Euclidean neighbors. The brain regions were illustrated in the BrainNet Viewer (http://www.nitrc.org/projects/bnv/).

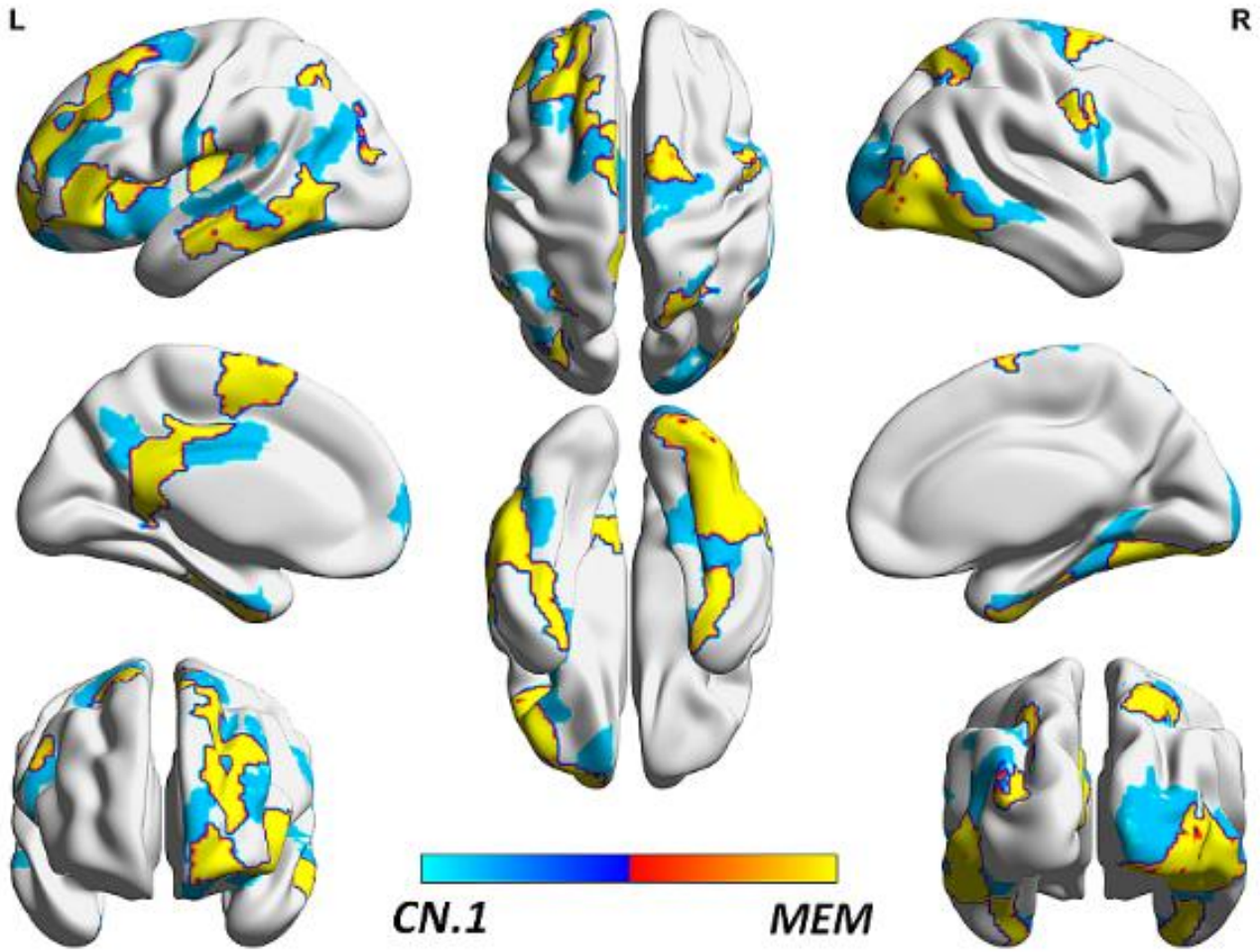

3.3 Network-level differences in hubness and segregation of HFA-memory regions and neighboring control nodes (region-effect), and between patients and controls (group-effect)

We sought to differentiate the network properties (segregation: AvgCC and hubness: AvgBC) in rsFC data of the MEM regions compared to the CNs, while simultaneously differentiating properties that differed in the epilepsy patients compared to controls. For each of the graph indices, we performed three separate ANOVAs involving a comparison between MEM

and different sets of CNs as a validation to ensure that any observed difference in segregation or hubness were related to actual memory encoding differences and not merely the choice of comparative CNs. ANOVAs on AvgBC revealed a significant main effect of region, with MEM having a lower AvgBC compared to CNs (MEM vs CN.1--, F's>14.16, FDR-p's $<3.4x10^{-3}$; MEM vs CN.2 -- F's> 20.16, FDR-p's $<2.8x10^{-4}$; MEM vs CN.RAND -- F's> 23.63, FDR-p's $<6.6x10^{-6}$). Neither the main effect of the group nor the interaction between group and region was significant in any of the models.

ANOVAs on AvgCC revealed a significant main effect for group, with patients having a lower AvgCC compared to controls (Patient vs Controls for MEM vs CN.1 -- F's> 8.2827, FDR-p's<0.004; Patient vs Controls for MEM vs CN.2 -- F's> 7.1628, FDR-p's <0.0088; Patient vs Controls for MEM vs CN.RAND -- F's> 8.1457, FDR-p's <0.007). Neither the main effect of the region (MEM vs CN.1, CN.2, and CN.RAND) nor the interaction between group and region was significant (Figure 3).

Figure 3: Network-level ANOVAs on AvgCC and AvgBC testing group-by-region effects

Composite network level (AvgCC and AvgBC) differences in MEM and CN (region-effect) between patients (PAT) and controls (CON) (group-effect). The black asterisks indicate that the main effects of group (for AvgCC) and the region (for AvgBC) were significant across network thresholds from 5-50%. Significant (Sig), * indicates the sparsity range in which the network differences are prominently different, yellow inset provides a magnified view of the difference in the AvgBC in the mid sparsity range.

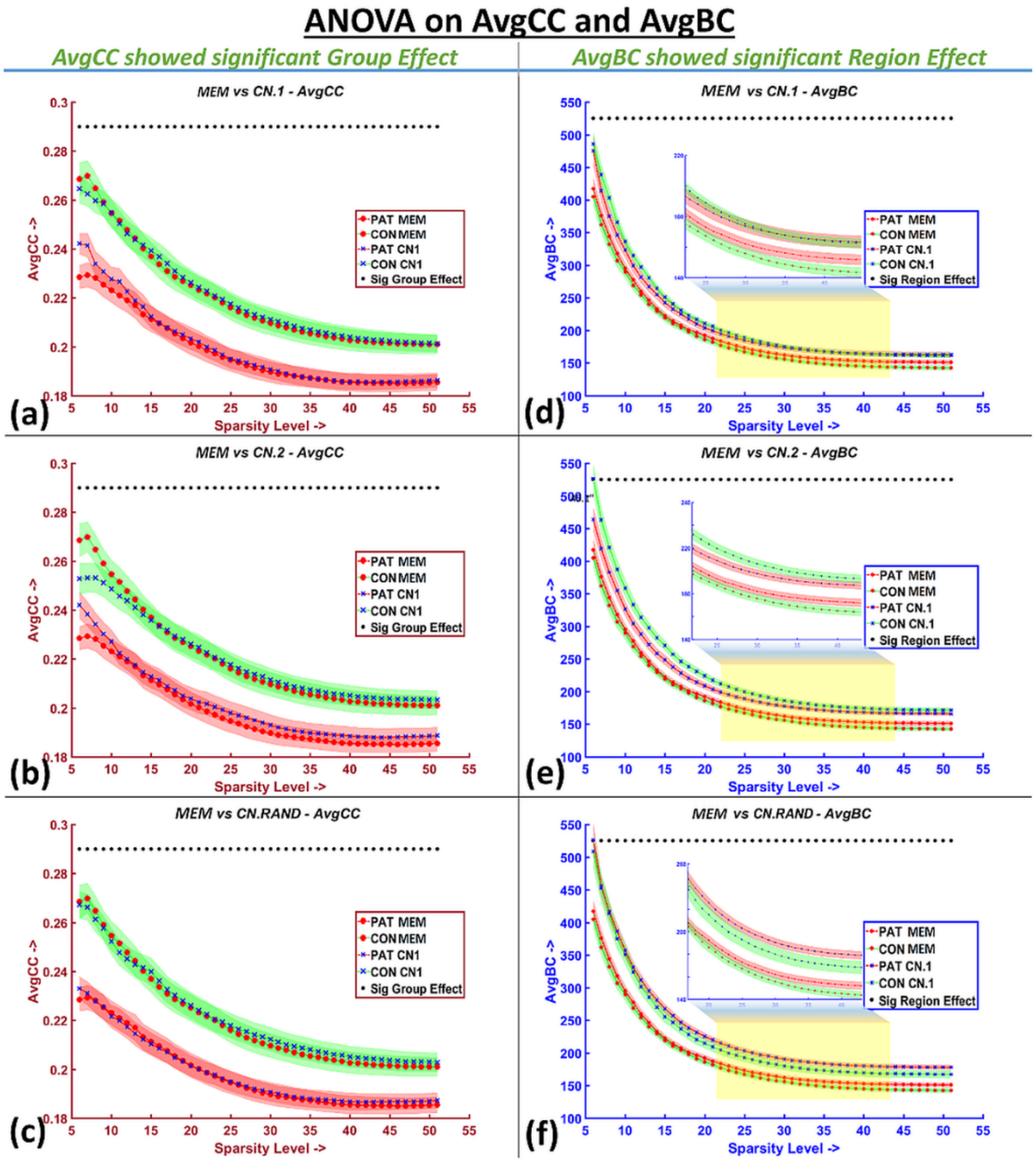
ANOVA on AvgCC and AvgBC
AvgCC showed significant Group Effect
AvgBC showed significant Region Effect
MEM vs CN.1 - AvgCC
MEM vs CN.2 - AvgCC
MEM vs CN.RAND - AvgCC
MEM vs CN.1 - AvgBC
MEM vs CN.2 - AvgBC
MEM vs CN.RAND - AvgBC
PAT MEM
CON MEM
PAT CN1
CON CN1
Sig Group Effect
PAT CN.1
CON CN.1
Sig Region Effect
AvgCC ->
AvgBC ->
Sparsity Level ->
(a)
(b)
(c)
(d)
(e)
(f)

3.4 Nodal-level differences in segregation and hubness of the HFA-memory regions and neighboring control nodes (region-effect), and between patients and controls (group-effect)

The above network-level analyses made clear that hubness differed between the MEM and CNs irrespective of group, while segregation differed between the groups irrespective of regional differences. Because such effects may hide differences at a nodal level. We applied similar ANOVAs to BC and CC estimated at the nodal level (NodalBC and NodalCC respectively).

ANOVAs on NodalBC revealed a significant main region-effect, revealing that NodalBC was reduced in MEM compared to CNs involving the left rostral middle frontal gyrus. The main effect of group and the group-by-region interaction was not significant (Table 3).

ANOVAs on NodalCC revealed a significant group-effect, revealing again that NodalCC was reduced in patients compared to controls across regions involving left caudal middle frontal gyrus, left inferior parietal gyrus, left precuneus, right fusiform, and lateral occipital gyri of the MEM (Table 3). Neither the main effect of the region nor the group-by-region interaction was significant.

Hence, both at the composite network and individual nodal level we found that hubness (BC) helps distinguish HFA-memory regions from their neighboring control regions, while segregation (CC) helps to distinguish patients from controls.

Table 3: ANOVAs on NodalCC or NodalBC testing group-by-region Effects.

NodalCC showed significant group-effect (patients had a lower NodalCC compared to controls irrespective of whether they were MEM or CNs). NodalBC showed significant region-effect (HFA-memory regions had lower NodalBC compared to CNs).

MAIN EFFECTS		
NodalCC (Significant group-effect: Patient vs Control)	**Fs**	**FDR-p's**
RLatOG.3	>5.9921	0.0057
RLatOG.4	>4.7211	0.0062
RFusG.1	>4.1904	0.0277
RFusG.2	>4.5526	0.0300
LSPG.3	>4.3929	0.0044
LITG.4	>4.2426	0.0136
NodalBC (Significant region-effect (MEM ROI's vs CN)		
LrMFG.4	>4.4909	0.0004

Regions of interest (ROIs), Clustering coefficient (CC), Betweenness Centrality (BC), HFA-Memory regions (MEM), Controls Nodes (CN) (Here we used the Boolean conjunction analysis to allow for only for those MEM regions significantly different between different comparisons with the three CN to be significant), F statistic of ANOVA (Fs), p values of ANOVA corrected for false discovery rate (pFDR), R.lateraloccipital (RLatOG), R.fusiform (RFusG), L.inferior temporal (LITG), L.superiorparietal (LSPG), L.rostralmiddlefrontal (LrMFG)

3.5 HFA-memory network decomposition among the established intrinsic networks

To help clarify the functional attributes of hubness that we uncovered about the HFA-memory network, we estimated the degree to which this network shared regions with well-established intrinsic networks (Figure 4a). For this, we estimated the percentage contribution of

the different intrinsic networks to the HFA-memory network (n.b., percentages avoids bias from the different number of ROI's that constitute each intrinsic network). We discovered that the HFA-memory network had a diverse "membership", sharing only modest overlap with any single intrinsic network, reflecting the complex set of cognitive and sensorimotor processes involved in effective memory encoding. For instance, the HFA-memory network comprised only 16% of the temporal lobe network regions (TN), 12% of the frontoparietal network (FPN), 14% of the dorsal attention network (DAN), and 13% of the cingulo-opercular network (COpN), amounting to a large 55% membership in what are often referred to as cognitive control systems (Figure 4a). This stands in contrast to very limited membership (15%) and overlaps with the task-negative default mode network (DMN), and 6% with the sensory-motor networks (SMN). The visual nature of verbal-memory encoding explains the overlap with the visual integration network (VIN, 24%) (Figure 4a). Noting that the HFA-memory regions do not constitute an intrinsic network, nor a surrogate for any one of them, we sought to determine if the BC of the HFA-memory network differed from that of the intrinsic networks. A repeated-measures ANOVA was performed to compare the AvgBC of the HFA-memory network with the AvgBC of the nine intrinsic networks. Due to the varying cognitive roles and responsibilities of these networks, it is reasonable to expect each intrinsic network would possess their own distinct range of BC scores. To test this, we assigned the brain parcels of the Lausanne's atlas as established by Gu et al, to nine well-established intrinsic, functional networks and ranked the networks according to their AvgBC values (Gu S, et al., 2015). These networks were of two broad categories, cognitive control systems (e.g., COpN, FPN, and DAN) and sensorimotor processing networks (e.g., SMN, VIN and AN). The HFA-memory network ranked 4th (AvgBC: 200±42) against the 9 intrinsic networks and differed significantly from all but one in AvgBC (Figure 4b and 5) (Supplementary Table 2a, b).

Figure 4: Nature of hubness of the HFA-memory network

(a) Pie-graph shows percent contribution of each intrinsic network to the HFA-memory network. (b) The bar graph in the second panel shows distinct optimal BC at which HFA-memory network operates in relation to the rest of the intrinsic networks. DMN and the FPN, which form the core hubs in the brain had the highest BC values. (c) The comparative bar graph shows the difference in BC of HFA member ROIs of an IN compared to BC of the other nodes in the same IN. (TN-temporal network, VIN-visual integrated network, SMN-sensorimotor network, DAN – dorsal attention network, COpN – cingulo-opercular network, FPN- frontoparietal network, DMN – default mode network). (d) The box and whisker plot shows the participation coefficient of the HFA-memory network in comparison with the different intrinsic networks.

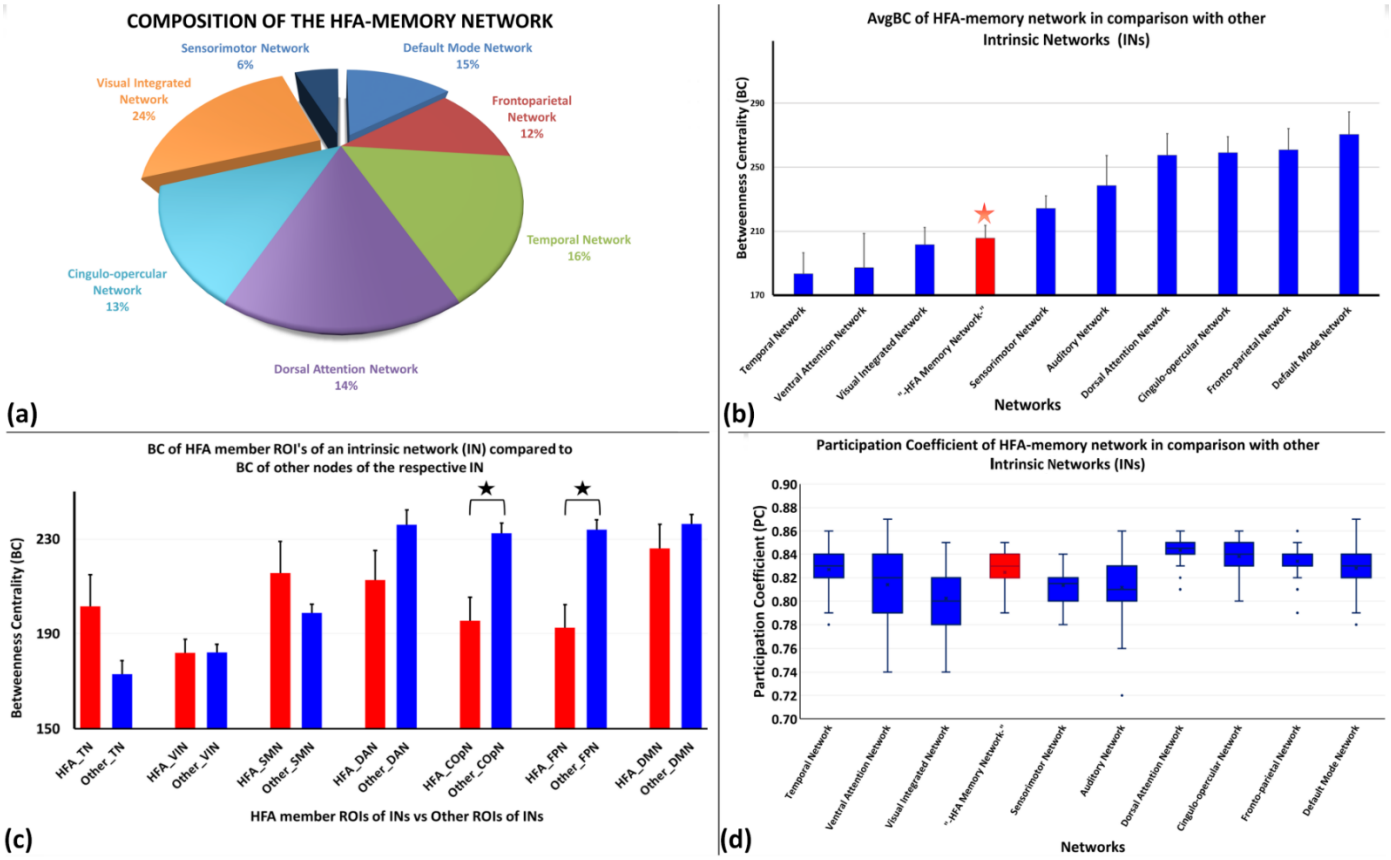

To further understand the nature of the overlap between intrinsic networks and the HFA-memory network, we tested whether the BC of ROIs of an intrinsic network that contributed to the HFA-memory regions differed from those that did not form a part of the HFA memory network. We found reliable differences only for the FPN (HFA_FPN vs Other_FPN: t=-3.63, $p=2.9x10^{-4}$) and COpN (HFA_COpN vs Other_COpN: t=-3.47, $p=5.2x10^{-4)}$, in each case revealing higher BC for the regions of intrinsic networks not part of the HFA-memory network (Figure 4c, Supplementary Table 3). Accordingly, the BC levels of HFA-memory regions involved in intrinsic networks (e.g., HFA_COpN and HFA_FPN) can be said to differ from the non-memory regions of these intrinsic networks (Other_COpN, Other_FPN). It was important to determine if this effect was driven by a patient vs control group difference. A two-way ANOVA showed that while the main effect of regional HFA status was significant (HFA_FPN vs Other_FPN: F=19.53, $p=1.9 x10^{-5}$; HFA_COpN vs Others_COpN: F=12.56, p=0.001), neither the main effect of group (patient vs control) nor the group-by-network interaction was significant (Supplementary Figure 6). The major finding was that cognitive control networks have a higher BC compared to the HFA-memory and sensorimotor processing networks.

Figure 5: ANOVA testing the difference in hubness of the different networks in the brain in comparison to the HFA-memory network

This matrix shows the difference in the hubness scores of the 9 intrinsic networks in comparison to the HFA memory network. While the HFA memory network appears to be a diverse, composite network with contributions from other INs. overall it does have a BC value distinct from 9 of the INs. In fact, with the exception of the DMN, all the INs display BC values distinct from at least 5 of the other INs. The values in the cells represent the significant comparisons of the post-hoc analysis of the ANOVA [Bonferroni corrected P-value <0.05 (Pcorr) was considered significant].

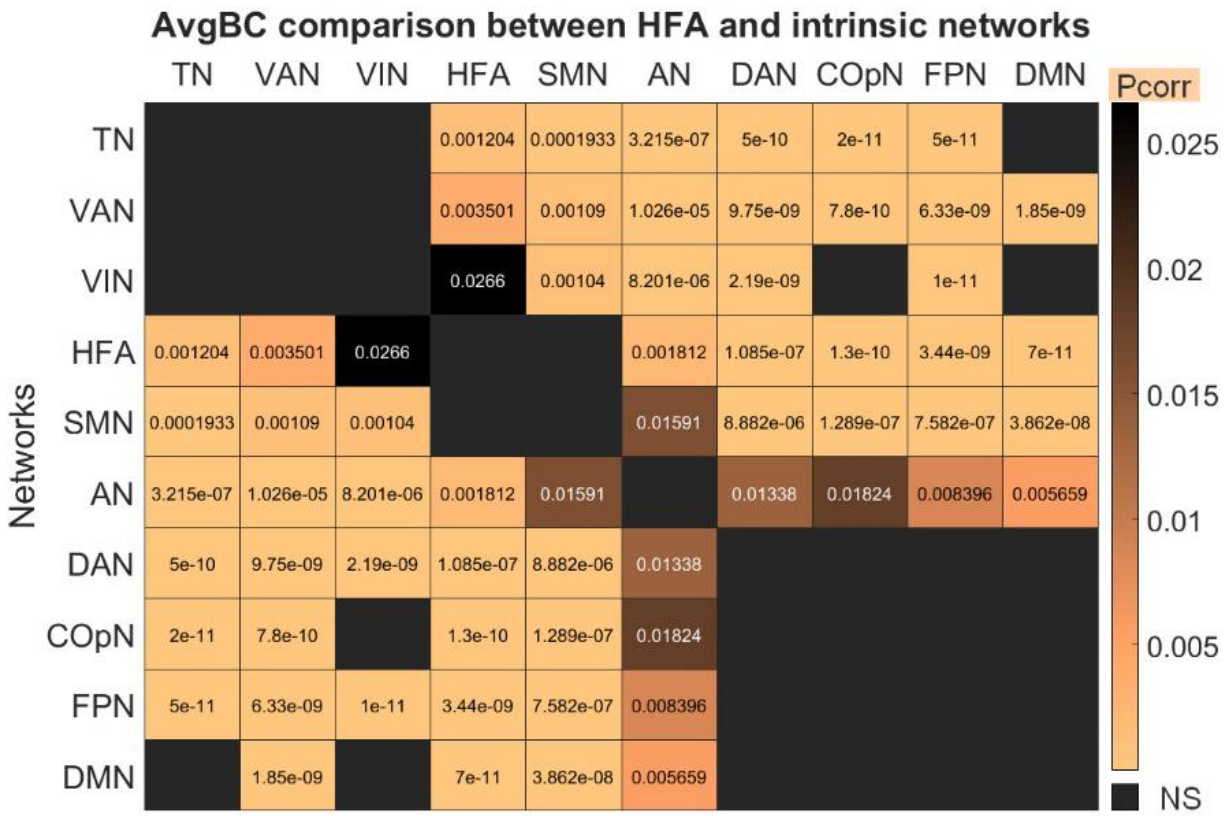

Having established the diverse membership of the HFA network, and the tendency of the INs to operate at different hubness levels, we next sought to verify the actual level of communication and interaction the HFA network displays with the intrinsic networks. To accomplish this, we defined the external connection of the HFA-memory network in relation to the different intrinsic networks through the use of a participation coefficient (AvgPC). Participation coefficient measures the extent to which regions within a network connect to networks other than its own, with a higher participation coefficient indicating that the regions connect with a variety of other networks. PC helps identify influential nodes in a network that are likely to be highly connected to other networks and, in turn, influence them. The cognitive control networks were found to have a higher AvgPC compared to the sensorimotor processing networks (Figure 4d and 7, Supplementary table 3a and b). Importantly, the HFA-memory network possessed AvgPC levels similar to that of the cognitive control networks, implying that along with its shared membership with these networks, inter-communication between the HFA-memory network and these control networks plays a major role in the implementation of memory encoding (Figure 4d, Supplementary table 3b).

3.6 Multivariate Machine Learning to Predict Verbal-memory Performance in Epilepsy Patients

Through both global and nodal analyses, we have established that in the resting-state the HFA-memory network is characterized by its hubness property and not regional segregation. As a final step, we wanted to test if either hubness or segregation were relevant to an individual's clinical memory performance. To accomplish this, random forest (RF) models were used to test the relationship between verbal-memory performance (CVLT-TL and P.REC) and the graph indices of HFA-memory regions (segregation and hubness). Though the two memory scores were

clinically related (CVLT-TL, total recall across five trials and P.REC, the average percent recall across all trials), they were not collinear (r=0.27, p=0.12). A regression RF model on CVLT-TL showed that NodalBC of four MEM variables significantly predicted CVLT-TL performance (Figure 6a: NodalBC of ROI 1 and 2 of RFusG, LITG, and LSFG). The model was found to be accurate, as we found that actual CVLT-TL scores were correlated with the predictions made with these four significant MEM NodalBC predictors (r=0.8, $p=2.04x10^{-8}$) (Figure 6c). A stepwise regression model (SRM) confirmed that among the 4 predictors, a linear model built with NodalBC of RFusG2 and LSFG6 emerged as significant predictors of CVLT-TL (F=10.599, dof=2, p=<0.0001: RFusG2-- beta= -0.53, t=-3.7, p=0.001, VIF=1.52; LSFG6-- beta=0.47, t=3.27, p=0.003, VIF=1.02).

The regression RF model on P.REC with the MEM NodalBC variables as predictors revealed six MEM variables with significant variable importance values (Figure 6b: NodalBC of LIstCinG, LrMFG, LITG, LIns, RLatOG, and RPreCG). We found that P.REC was significantly correlated with the predictions made with these six significant MEM NodalBC measures (r=0.88, $p=2.14x10^{-11}$; Figure 6d), indicating that the RF model was accurate. An SRM model testing the six predictors with P.REC produced no significant predictors. Thus, the RF method produced a more sensitive and complex model of the relationship between hubness and memory performance, likely stemming from the fact that SRM only detects linear, not non-linear, relationships, noting that RF captures both.

In the RF models with the MEM NodalCC as predictors, none of the NodalCC measures were deemed significant in >95% of the permutations. Thus, none of these variables demonstrated a reliable ability to predict either P.REC or CVLT-TL performance.

This modeling work established that resting-state hubness of the HFA-memory regions not only predicted the verbal-memory performance during the IEEG testing, but also baseline levels of neuropsychological memory. Regional segregation showed no relation to either of these memory performances.

Figure 6: Random Forest Models to establish a relationship between hubness and verbal-memory performance

Random forest models help establish both linear and non-linear relationships between predictors and response. (a) BC of the HFA-memory regions (MEM) were used to predict CVLT-TL. The BC of the MEM were sorted by the number of times they were selected as a significant predictor based on 1000 permutations of the random forest (RF) model. LITG, LSFG, and RFusG were significantly associated with the CVLT-TL performance, (b) BC of the HFA-memory regions (MEM) were used to predict P.REC. The BC of the MEM were sorted by the number of times they were selected as a significant predictor based on 1000 permutations of the RF model. LIstCingG, LrMFG, LITG, LIns, RLatOG, and RPreCG were significantly associated with the P.REC memory performance. (c) Prediction of CVLT-TL performance made with BC of the MEM ROIs, (d) Prediction of P.REC performance during IEEG monitoring made with BC of the MEM ROIs. Measures exceeding beyond the blue line (the blue line indicates the $p<0.05$ threshold, below which none are considered significant). California verbal learning test (CVLT), number of times selected in the RF model (N), Betweenness Centrality (BC), High-Frequency Activity (HFA), correlation coefficient (r), probability value (p).

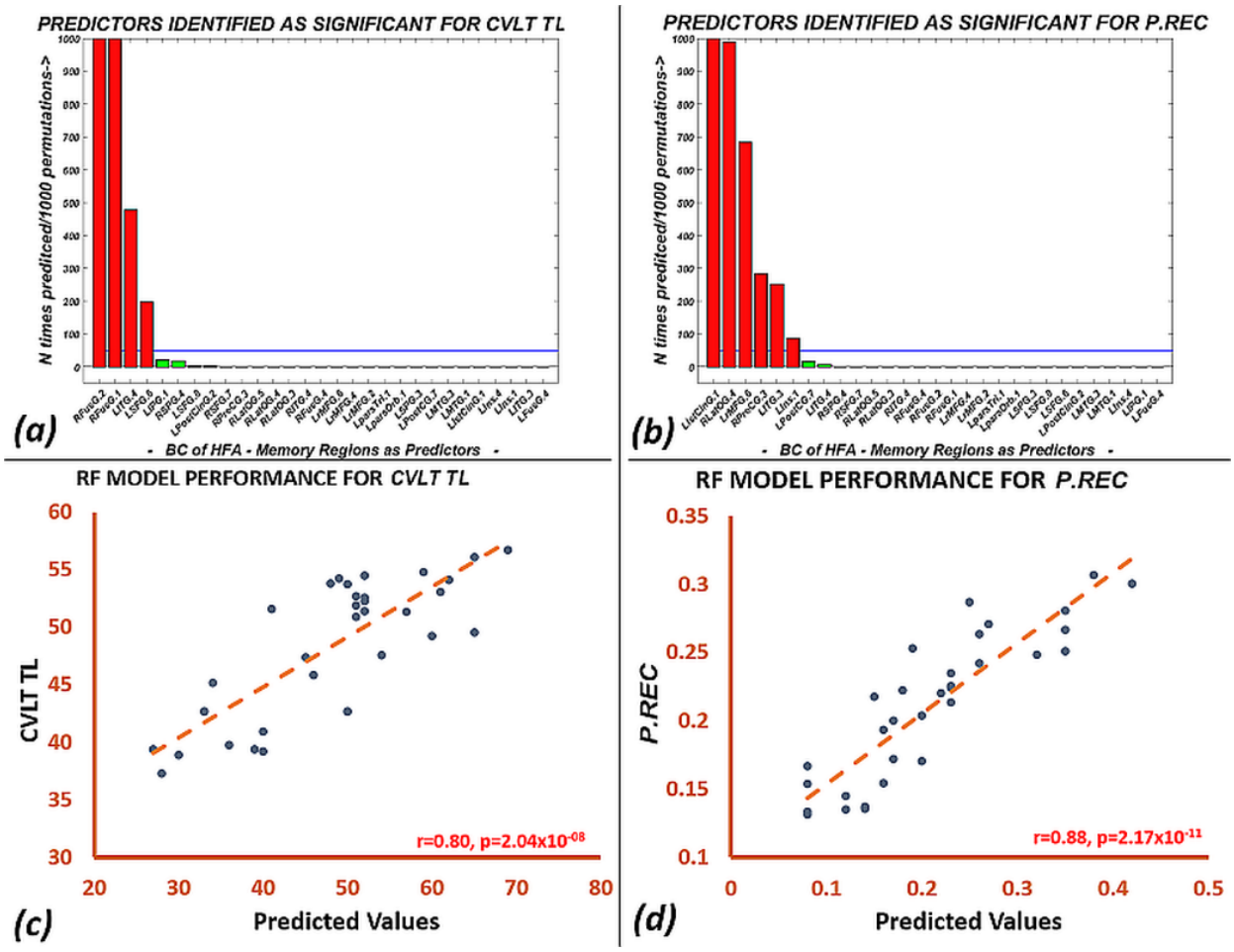

4 DISCUSSION

A fundamental question in network neuroscience regards the specific relationship between intrinsic network architecture and task-defined regional brain activity. Thus, the goal of this study was to focus on the understanding of the broader network features that underlie and support memory functionality, particularly when such functionality is defined through a regionally limited and sparse technology such as IEEG. We demonstrated that by integrating spectral markers of memory encoding (HFA) with rsfMRI data, one can identify network features of an IEEG-derived

verbal-memory network. This method also allowed us to reveal the diversity of memory encoding operations by revealing the contributions of multiple functional networks to successful memory. Given the inherent presence of a diseased sample when using IEEG data, we tested the generality of our findings by determining if the observed memory encoding network characteristics, as embedded in resting-state data, were similar in DRE patients and healthy controls. To assess the clinical validity of these memory network characteristics, we tested whether these characteristics were associated with actual, baseline verbal-memory performance. In summary, with a combined IEEG-rsfMRI approach, we were able to layout the network characteristics and multifaceted intrinsic cognitive components associated with successful verbal-memory encoding.

The data demonstrates that BC, a measure of hubness, as opposed to CC, a measure of segregation, is important for driving memory-encoding networks toward successful recall. Studies have indicated that in the human brain, the highest hub scores localize in the DMN and FPNs (Power JD, et al., 2013;van den Heuvel MP et al., 2013). (Cole MW et al., 2013;van den Heuvel MP, et al., 2013), a finding consistent with our data. Compared to these dominant networks in the brain, we found that the HFA-memory network had a lower hub score, but nonetheless a level of hubness that sustained and supported successful memory encoding during IEEG testing. The apparent lower hub score for the HFA-memory network (i.e., AvgBC of MEM vs CN), appeared to emerge from the fact that the control nodes with which they were compared were located in regions with hierarchically higher hub scores. While there have been studies showing the hippocampus to be a part of the brain's hub architecture (Van Den Heuvel MP et al., 2011), there has been no study outside of this current data to show, one, the distinctiveness of the hub score (AvgBC) of a memory network and, two, it's standing relative to the hubness values of other cognitive control networks.

The hubness value of the HFA-memory network was not related to the presence of epilepsy, and was obtained in the setting of normative baseline memory scores. As a point of contrast, we show that the DRE patients and healthy controls differed with respect to the regional segregation (CC) of both the HFA-memory network and their neighboring control nodes. This segregation effect appeared to be a consequence of epileptic pathophysiology, a finding consistent with the previous literature (Haneef Z et al., 2014).

Nodal hubness and segregation mirrored the above composite network findings. During the estimation of memory encoding during IEEG testing, we excluded electrodes and regions that were a part of the clinically hypothesized epileptogenic zone in order to avoid the effect of epileptic interictal and ictal discharges on the estimation of HFA-memory regions, both in terms of affecting a patient's ability to encode words, as well as the power changes related to the epileptic discharges in IEEG data. This is in accord with previous studies which have shown that significantly altered BC localized and lateralized to the epileptogenic regions in both IEEG and rsFC (Haneef Z, et al., 2014;Wilke C et al., 2011). Excluding those regions from analysis helped establish that the region-effects we observed at both the network level (AvgBC) and nodal level (NodalBC) were, indeed, associated with successful encoding. Note, in the setting of intact CVLT–TL performance, the appearance of regional AvgBC effects points to the likelihood that the various HFA-memory regions work in unison to maintain the integrity of verbal-memory encoding. The positive relationship we observed in the RF model between task positive, cognitive control regions and stronger memory performance is evidence of the way cognitive control benefits memory. The negative relationship seen between some NodalBC values and memory performance is less clear. On this point, there is literature showing that the areas involved in the early stages of memory encoding such as the ventral attention stream (i.e., RFUSG2) may be de-activated later in the

memory encoding process (Burke JF, et al., 2015). Unfortunately, the low temporal resolution of rsfMRI would blur and be insensitive to this shift in activity, potentially leading to a negative correlation.

To clarify further the nature of the HFA-memory hubness findings, we compared the BC of the HFA-memory network to well-known intrinsic networks. In work utilizing network controllability measures, Gu and colleagues (Gu S, et al., 2015) argued that the controllability of each of the intrinsic networks is unique. Applying this concept to the hubness results, we did see that the different cognitive networks operated at different hubness levels even in the resting-state. (n.b., the same networks examined by Gu et al. 2015).

Importantly, we noted that the membership of different intrinsic networks in the HFA-memory network makes clear that the HFA-memory network utilizes a diverse set of intrinsic functionalities to drive successful verbal-memory encoding. The HFA-memory network has major membership (55%) from cognitive controls systems that call upon attentional resources (DAN), lexical/semantic processing and memory consolidation (TN), and top-down control of executive functions (FPN, trial-specific control and selective attention; COpN, control of overall task goals and error monitoring) (Vaden KI, Jr. et al., 2013). Interestingly, we found that the HFA-memory regions that share membership with the intrinsic networks tend to operate at the same level of hubness as other constituents of the intrinsic network, with the exception of FPN and COpN networks (Figure 4c). These members of the HFA-memory network had a lower BC. (Sheffield JM et al., 2015). Other HFA-memory regions, utilizing cognitive processes that are part of other intrinsic networks, appear to operate at hubness levels that are comparable and optimal for the intrinsic networks as a whole (Figure 4c). Thus, out data indicates that effective memory encoding is not dominated by a central cognitive core, but is the result of a diverse set of componential

functions distributed across multiple intrinsic networks, largely involving task-positive networks, all toward the goal of maximizing subsequent recall. This distribution across multiple regions is likely reflective of adaptive "associative" encoding, consistent with the extensive literature showing that recruitment of multiple cognitive and sensory processes is a crucial feature of an effective memory (Cowan N, 2017;Tulving E et al., 1996).

In order to go beyond a basic demonstration of the functional diversity of the HFA-memory network through data showing regional overlap, we investigated the interaction of the HFA-memory network with the different intrinsic brain networks. Participation coefficient analysis showed that regions of the HFA-memory network connect with a diverse set of intrinsic networks, participating at a level higher than the VIN, AN, SMN which constitute the sensorimotor processing systems. The HFA-memory network operates at a level of AvgPC comparable to TN and DMN, though lower than the FPN, COpN and DAN, implying that the HFA-memory network communicates intensively with the cognitive control networks to achieve effective memory.

Lastly, we verified through RF modelling that the hubness of selected HFA-memory regions were significantly associated with both baseline verbal-memory performance (CVLT-TL) and successful recall during simultaneous IEEG-memory encoding (P.REC). The regions found to be predictive of memory performance are consistent with literature showing language and executive function processes (working memory, attention) mediate memory encoding, with such processes bringing semantic associations to bear during memory engram formation or utilizing a "central executive" to manipulate incoming information in working memory (Gutchess AH et al., 2005). Thus, similar to the data looking at the overlap with the intrinsic networks, the RF model pointed to the multivariate nature of memory encoding. Indeed, learning during the trials of the CVLT can be achieved through auditory attention and very short-term "holding" and covert verbal

recitation of the information, i.e., good performance does not require long-term memory storage. The fact that this involved mostly left as opposed to right hemisphere regions could potentially point to a material-specific effect related to the word lists and covert verbal processing (Campoy G, 2008;Cowan N, 2008). Overall, our data shows that the hubness of regions matters more than segregation for the prediction of both baseline verbal-memory encoding abilities and successful recall following periods of HFA-associated memory encoding activity.

The two modalities we use, IEEG and rsfMRI, measure two biologically and technically unrelated signals (direct activity of neuronal ensembles and metabolic-rate-driven synchronous fluctuations in cerebral-blood-flow, respectively), each based on very different spatio-temporal scales. We employed a method of using the IEEG HFA derived memory regions in individual subjects and transforming them into a cortex-based intrinsic functional connectivity patterns. The advantage of such an integrated technique is multifold. First, from a statistical viewpoint, isolating HFA-memory regions allowed us to avoid, in both the inter- and intra-group comparisons, a large number of brain regions that are unassociated with memory encoding, reducing the chances of Type I error. The multiple comparisons performed in this study were restricted to the 29 regions and their corresponding controls regions, as opposed to correcting for ROIs of the entire Lausanne's atlas. Second, the method of building a 'Super-Brain' allowed us to take advantage of the fine-grained temporal sequencing of cognitive events in IEEG, and reduce but not eliminate the problem of sparse spatial sampling. The use of a 'Super Brain' is widely established in cognitive studies to map reliable networks associated with memory encoding and retrieval (Greenberg JA, et al., 2015;Kragel JE, et al., 2017). Third, IEEG is a spatially constrained investigative modality (i.e., sparse sampling). However, integration of the data with a modality such as rsfMRI allowed for evaluation of function throughout the brain even if patients were not

implanted in those regions. This advantage has been exploited in previous studies involving isolation of the epileptogenic zone (Aghakhani Y et al., 2015), and in establishing task related BOLD-gamma relations (Esposito F, et al., 2013). Fourth, this type of integration opened up the door to studying the correspondence between BOLD signal changes and different frequency ranges, along with their linked behavioral activity. Indeed, linkages between neuronal synchrony and cognitive functions may be highly specific to the frequencies in which they occur. For instance, sensorimotor functions are regulated by beta synchrony (Brovelli A et al., 2004), and the correspondence between BOLD response and visual and auditory IEEG activity is regulated by synchrony (Esposito F, et al., 2013). Among the many different frequencies that can be studied in the IEEG, there has consistently been a close correspondence of the gamma band component of the local field potentials in the cerebral cortex with the BOLD signal for different motor, sensory and cognitive neuronal functions (Lachaux JP et al., 2007). Our results are certainly another example of this correspondence.

A handful of studies have performed network analysis directly on memory task-IEEG signals, studying the network synchrony present during encoding process (Burke JF et al., 2013;Solomon EA, et al., 2017;Vecchio F et al., 2016). Such studies have emphasized different properties of the gamma frequency band-width, including spectral power changes, phase locking value, and exact low resolution topographical analysis (eLORETA). These studies have found that increased gamma spectral power, asynchronous gamma oscillations coupled with synchronous theta and increased gamma-smallworldness, were associated with better verbal and non-verbal episodic memory performance. Solomon et al., examined high gamma during verbal-memory and observed both synchronous and asynchronous activity. They found that regions in frontal, temporal, and medial temporal lobe cortex asynchronous with other regions, displayed a high level

of connection strength, implying a high level of centrality or hubness within the memory network, a finding broadly consistent with the current results (Solomon EA, et al., 2017). Our study, however, adds to the literature by showing that through repetitive processes of memory encoding, gamma frequency activity can establish synchrony to the point that even slow moving resting-state BOLD fluctuations reflect their network impact. This network impact can be best characterized as establishing a level of hubness distinct from other INs, yet spatially overlapping several INs, particularly those involved in cognitive control. In the first study of its kind, applying an integrated IEEG-fMRI method, we have shown that established markers of memory encoding correspond to meaningful network differences captured by rsfMRI. In clinical terms, knowing a region is a hub, playing an important role in multi-regional and multi-functional connectivity, may inform technologies trying to identify the most effective targets to electrically or pharmacologically stimulate for cognitive enhancement in areas such as memory (Ezzyat Y et al., 2017;Ezzyat Y et al., 2018;Kucewicz MT et al., 2018), or perhaps be used to identify the areas with sufficient influence over targets to generate effective neurofeedback loops (Hohenfeld C et al., 2017;Murphy AC et al., 2017). Lastly, in the setting of clinical disorders such as epilepsy, knowledge of the broader functional network in which a given region is embedded, both its proximity to the seizure onset zone (Horak PC et al., 2017;Towgood K et al., 2015), and the degree to which it operates as a core hub of the functional network, may contribute to the risk/benefit calculus of resecting a region, essentially allowing clinicians to better account for the network context and behavioral/cognitive impact of surgery.

In terms of the limitations of this study, the hippocampus was not significant for SME because it was found that in 11 of 37 subjects hippocampal electrodes were excluded from analysis as they were part of the seizure onset zone or interictal zone, though they constitute an important

part of the episodic memory network. Electrodes with higher epileptiform activity from regions such as the hippocampus, which is known to be involved episodic memory, were not included in the analyses, and the few electrodes that remained in these regions were not statistically significant for HFA. (Supplementary figure 8)(Yarkoni T et al., 2011). Note, the clinical memory performance of this cohort of DRE patients was within the normal range making the point that while the hippocampus is a crucial structure in memory encoding, it's actually the entire network associated with encoding that maintains the integrity of the function. We also want to acknowledge that there are a large number of network centrality measures, each with their own sensitivities to aspects of network architecture. Betweenness centrality has the assumption that short paths lengths are an important part of centrality, and that a region inter-connecting or "between" the separate modules is important, leaving open the question as to whether the BC hub itself is actually densely connected.

Conclusion:

In conclusion, the present study establishes that IEEG integrated with rsfMRI is a useful method for establishing the network characteristics associated with cognitive processes such as verbal-memory encoding. By combining group-level 'IEEG-derived-memory' findings with individual level rsfMRI data, we showed that repetitive gamma band frequency activity can establish synchrony to the point that even slow moving resting-state BOLD fluctuations reflect their network impact. Through this methodology, we were able to characterize key network features of HFA-memory related activity and demonstrate the integrative role played by other intrinsic cognitive networks. Accordingly, we have extended the field's understanding of HFA-memory-related activity beyond statements of isolated, regional functionality. By decomposing the HFA-memory network into its intrinsic cognitive components we were able to demonstrate

that effective verbal-memory encoding is not dominated by a central cognitive core, but is the result of a complex set of computational functions distributed across multiple intrinsic networks. We show that the HFA-memory network operates at distinct hubness levels, as do other intrinsic networks, all toward the goal of maximizing subsequent verbal recall, thereby clarifying the conditions of the baseline, tonic state that support effective, phasic, task-dependent memory encoding. We also verify that this trait-like network feature holds true for both epilepsy patients and healthy controls. We show that hubness matters more than segregation for the prediction of both baseline verbal-memory encoding success and recall following periods of HFA-associated memory encoding. Lastly, our DRE patients possessed intact episodic memory encoding and comprised a sample with regionally diverse epileptiform dysfunction. In this context, our data can be seen as displaying the diverse set of regional hubness levels and functionalities potentially available to support effective memory encoding through compensatory brain reorganization.

Author Contributions

Conceptualization and design of the study was by GC, JIT and XH**.** The clinical evaluation and enrollment of patients in the EMU was by MS. The surgical procedures were headed and performed by AS. The neuropsychology data was collected and analyzed by NS, XH, and GC. IEEG and neuroimaging data were analyzed by GC, JK, WH, YE and XH. Interpretation of results, drafting the manuscript and critical revisions were done by CG, XH, JK, WH, AS, MS and JIT. JIT in the capacity of corresponding author agrees to be accountable for all aspects of the work, ensuring the accuracy or integrity of any part of the work investigated and resolved.

Acknowledgement

The authors thank the Epilepsy Monitoring Unit their help in data acquisition. We thank Dr. Dorian Pustina for his help with the machine learning strategy. The authors thank all the healthy controls and patients with epilepsy, whose data was used for this study. This work was supported by the DARPA Restoring Active Memory (RAM) program (Cooperative Agreement N66001-14-2-4032). JIT acknowledges partial support from NIMH R01-MH104606. The views, opinions, and/or findings contained in this material are those of the authors and should not be interpreted as representing the official views or policies of the Department of Defense or the U.S. Government.

Disclosure of Conflicts of Interest

The authors declare that the research was conducted in the absence of any commercial or financial relationships that could be construed as a potential conflict of interest.

Supplementary material

Supplementary material is available online.

References

Aghakhani Y, Beers CA, Pittman DJ, Gaxiola-Valdez I, Goodyear BG, Federico P (2015), Co-localization between the BOLD response and epileptiform discharges recorded by simultaneous intracranial EEG-fMRI at 3 T. Neuroimage Clin 7:755-763.

Alexander-Bloch AF, Gogtay N, Meunier D, Birn R, Clasen L, Lalonde F, Lenroot R, Giedd J, et al. (2010), Disrupted modularity and local connectivity of brain functional networks in childhood-onset schizophrenia. Frontiers in systems neuroscience 4:147.

Altmann A, Tolosi L, Sander O, Lengauer T (2010), Permutation importance: a corrected feature importance measure. Bioinformatics 26:1340-1347.

Axmacher N, Schmitz DP, Wagner T, Elger CE, Fell J (2008), Interactions between medial temporal lobe, prefrontal cortex, and inferior temporal regions during visual working memory: a combined intracranial EEG and functional magnetic resonance imaging study. J Neurosci 28:7304-7312.

Breiman L (2001), Random forests. Machine learning 45:5-32.

Brovelli A, Ding M, Ledberg A, Chen Y, Nakamura R, Bressler SL (2004), Beta oscillations in a large-scale sensorimotor cortical network: directional influences revealed by Granger causality. Proc Natl Acad Sci U S A 101:9849-9854.

Burke JF, Ramayya AG, Kahana MJ (2015), Human intracranial high-frequency activity during memory processing: neural oscillations or stochastic volatility? Curr Opin Neurobiol 31:104-110.

Burke JF, Zaghloul KA, Jacobs J, Williams RB, Sperling MR, Sharan AD, Kahana MJ (2013), Synchronous and asynchronous theta and gamma activity during episodic memory formation. Journal of Neuroscience 33:292-304.

Burke JF, Zaghloul KA, Jacobs J, Williams RB, Sperling MR, Sharan AD, Kahana MJ (2013), Synchronous and asynchronous theta and gamma activity during episodic memory formation. J Neurosci 33:292-304.

Burns SP, Santaniello S, Yaffe RB, Jouny CC, Crone NE, Bergey GK, Anderson WS, Sarma SV (2014), Network dynamics of the brain and influence of the epileptic seizure onset zone. Proc Natl Acad Sci U S A 111:E5321-5330.

Campoy G (2008), The effect of word length in short-term memory: Is rehearsal necessary? Q J Exp Psychol (Hove) 61:724-734.

Cole MW, Reynolds JR, Power JD, Repovs G, Anticevic A, Braver TS (2013), Multi-task connectivity reveals flexible hubs for adaptive task control. Nat Neurosci 16:1348-1355.

Cowan N (2008), What are the differences between long-term, short-term, and working memory? Prog Brain Res 169:323-338.

Cowan N (2017), The many faces of working memory and short-term storage. Psychon Bull Rev 24:1158-1170.

Esposito F, Singer N, Podlipsky I, Fried I, Hendler T, Goebel R (2013), Cortex-based inter-subject analysis of iEEG and fMRI data sets: application to sustained task-related BOLD and gamma responses. Neuroimage 66:457-468.

Ezzyat Y, Kragel JE, Burke JF, Levy DF, Lyalenko A, Wanda P, O'Sullivan L, Hurley KB, et al. (2017), Direct Brain Stimulation Modulates Encoding States and Memory Performance in Humans. Curr Biol 27:1251-1258.

Ezzyat Y, Wanda PA, Levy DF, Kadel A, Aka A, Pedisich I, Sperling MR, Sharan AD, et al. (2018), Closed-loop stimulation of temporal cortex rescues functional networks and improves memory. Nat Commun 9:365.

Fahoum F, Lopes R, Pittau F, Dubeau F, Gotman J (2012), Widespread epileptic networks in focal epilepsies: EEG-fMRI study. Epilepsia 53:1618-1627.

Geller AS, Schlefer IK, Sederberg PB, Jacobs J, Kahana MJ (2007), PyEPL: a cross-platform experiment-programming library. Behav Res Methods 39:950-958.

Genovese CR, Lazar NA, Nichols T (2002), Thresholding of statistical maps in functional neuroimaging using the false discovery rate. Neuroimage 15:870-878.

Greenberg JA, Burke JF, Haque R, Kahana MJ, Zaghloul KA (2015), Decreases in theta and increases in high frequency activity underlie associative memory encoding. Neuroimage 114:257-263.

Gu S, Pasqualetti F, Cieslak M, Telesford QK, Yu AB, Kahn AE, Medaglia JD, Vettel JM, et al. (2015), Controllability of structural brain networks. Nat Commun 6:8414.

Gutchess AH, Welsh RC, Hedden T, Bangert A, Minear M, Liu LL, Park DC (2005), Aging and the neural correlates of successful picture encoding: frontal activations compensate for decreased medial-temporal activity. J Cogn Neurosci 17:84-96.

Hagmann P, Cammoun L, Gigandet X, Meuli R, Honey CJ, Wedeen VJ, Sporns O (2008), Mapping the structural core of human cerebral cortex. PLoS biology 6:e159.

Haneef Z, Chiang S (2014), Clinical correlates of graph theory findings in temporal lobe epilepsy. Seizure 23:809-818.

Hohenfeld C, Nellessen N, Dogan I, Kuhn H, Muller C, Papa F, Ketteler S, Goebel R, et al. (2017), Cognitive Improvement and Brain Changes after Real-Time Functional MRI Neurofeedback Training in Healthy Elderly and Prodromal Alzheimer's Disease. Front Neurol 8:384.

Horak PC, Meisenhelter S, Song Y, Testorf ME, Kahana MJ, Viles WD, Bujarski KA, Connolly AC, et al. (2017), Interictal epileptiform discharges impair word recall in multiple brain areas. Epilepsia 58:373-380.

Humphries MD, Gurney K, Prescott TJ (2006), The brainstem reticular formation is a small-world, not scale-free, network. Proceedings Biological sciences / The Royal Society 273:503-511.

Jacques C, Witthoft N, Weiner KS, Foster BL, Rangarajan V, Hermes D, Miller KJ, Parvizi J, et al. (2016), Corresponding ECoG and fMRI category-selective signals in human ventral temporal cortex. Neuropsychologia 83:14-28.

Jensen O, Kaiser J, Lachaux J-P (2007), Human gamma-frequency oscillations associated with attention and memory. Trends in neurosciences 30:317-324.

Jin SH, Jeong W, Chung CK (2015), Mesial temporal lobe epilepsy with hippocampal sclerosis is a network disorder with altered cortical hubs. Epilepsia 56:772-779.

Kaiser M, Hilgetag CC (2006), Nonoptimal component placement, but short processing paths, due to long-distance projections in neural systems. PLoS computational biology 2:e95.

Khursheed F, Tandon N, Tertel K, Pieters TA, Disano MA, Ellmore TM (2011), Frequency-specific electrocorticographic correlates of working memory delay period fMRI activity. Neuroimage 56:1773-1782.

Kragel JE, Ezzyat Y, Sperling MR, Gorniak R, Worrell GA, Berry BM, Inman C, Lin JJ, et al. (2017), Similar patterns of neural activity predict memory function during encoding and retrieval. Neuroimage 155:60-71.

Kucewicz MT, Berry BM, Miller LR, Khadjevand F, Ezzyat Y, Stein JM, Kremen V, Brinkmann BH, et al. (2018), Evidence for verbal memory enhancement with electrical brain stimulation in the lateral temporal cortex. Brain 141:971-978.

Lachaux JP, Fonlupt P, Kahane P, Minotti L, Hoffmann D, Bertrand O, Baciu M (2007), Relationship between task-related gamma oscillations and BOLD signal: new insights from combined fMRI and intracranial EEG. Hum Brain Mapp 28:1368-1375.

Lega B, Burke J, Jacobs J, Kahana MJ (2014), Slow-theta-to-gamma phase–amplitude coupling in human hippocampus supports the formation of new episodic memories. Cerebral Cortex 26:268-278.

Liaw A, Wiener M (2002), Classification and regression by random-Forest. Rnews 2:18-22.

Logothetis NK, Pauls J, Augath M, Trinath T, Oeltermann A (2001), Neurophysiological investigation of the basis of the fMRI signal. Nature 412:150-157.

Long NM, Burke JF, Kahana MJ (2014), Subsequent memory effect in intracranial and scalp EEG. Neuroimage 84:488-494.

Mizuhara H (2012), Cortical dynamics of human scalp EEG origins in a visually guided motor execution. Neuroimage 62:1884-1895.

Mizuhara H, Wang L-Q, Kobayashi K, Yamaguchi Y (2005), Long-range EEG phase synchronization during an arithmetic task indexes a coherent cortical network simultaneously measured by fMRI. Neuroimage 27:553-563.

Murphy AC, Bassett DS (2017), A Network Neuroscience of Neurofeedback for Clinical Translation. Curr Opin Biomed Eng 1:63-70.

Murta T, Chaudhary U, Tierney TM, Dias A, Leite M, Carmichael DW, Figueiredo P, Lemieux L (2017), Phase–amplitude coupling and the BOLD signal: a simultaneous intracranial EEG (icEEG)-fMRI study in humans performing a finger-tapping task. Neuroimage 146:438-451.

Powell HW, Richardson MP, Symms MR, Boulby PA, Thompson PJ, Duncan JS, Koepp MJ (2007), Reorganization of verbal and nonverbal memory in temporal lobe epilepsy due to unilateral hippocampal sclerosis. Epilepsia 48:1512-1525.

Power JD, Schlaggar BL, Lessov-Schlaggar CN, Petersen SE (2013), Evidence for hubs in human functional brain networks. Neuron 79:798-813.

Rubinov M, Sporns O (2010), Complex network measures of brain connectivity: uses and interpretations. Neuroimage 52:1059-1069.

Rugg MD, Otten LJ, Henson RN (2002), The neural basis of episodic memory: evidence from functional neuroimaging. Philos Trans R Soc Lond B Biol Sci 357:1097-1110.

Sheffield JM, Repovs G, Harms MP, Carter CS, Gold JM, MacDonald AW, 3rd, Daniel Ragland J, Silverstein SM, et al. (2015), Fronto-parietal and cingulo-opercular network integrity and cognition in health and schizophrenia. Neuropsychologia 73:82-93.

Solomon EA, Kragel JE, Sperling MR, Sharan A, Worrell G, Kucewicz M, Inman CS, Lega B, et al. (2017), Widespread theta synchrony and high-frequency desynchronization underlies enhanced cognition. Nat Commun 8:1704.

Sperling MR, O'Connor MJ, Saykin AJ, Plummer C (1996), Temporal lobectomy for refractory epilepsy. JAMA 276:470-475.

Towgood K, Barker GJ, Caceres A, Crum WR, Elwes RD, Costafreda SG, Mehta MA, Morris RG, et al. (2015), Bringing memory fMRI to the clinic: comparison of seven memory fMRI protocols in temporal lobe epilepsy. Hum Brain Mapp 36:1595-1608.

Tracy J, Pustina D, Doucet G, Osipowicz K (2014), Seizure-induced neuroplasticity and cognitive network reorganization in epilepsy. Cognitive Plasticity in Neurologic Disorders:29.

Tracy JI, Doucet GE (2015), Resting-state functional connectivity in epilepsy: growing relevance for clinical decision making. Curr Opin Neurol 28:158-165.

Tulving E, Markowitsch HJ, Craik FE, Habib R, Houle S (1996), Novelty and familiarity activations in PET studies of memory encoding and retrieval. Cereb Cortex 6:71-79.

Vaden KI, Jr., Kuchinsky SE, Cute SL, Ahlstrom JB, Dubno JR, Eckert MA (2013), The cingulo-opercular network provides word-recognition benefit. J Neurosci 33:18979-18986.

Van Den Heuvel MP, Sporns O (2011), Rich-club organization of the human connectome. Journal of Neuroscience 31:15775-15786.

van den Heuvel MP, Sporns O (2013), Network hubs in the human brain. Trends Cogn Sci 17:683-696.

van Diessen E, Diederen SJ, Braun KP, Jansen FE, Stam CJ (2013), Functional and structural brain networks in epilepsy: what have we learned? Epilepsia 54:1855-1865.

Vecchio F, Miraglia F, Quaranta D, Granata G, Romanello R, Marra C, Bramanti P, Rossini PM (2016), Cortical connectivity and memory performance in cognitive decline: A study via graph theory from EEG data. Neuroscience 316:143-150.

Wilke C, Worrell G, He B (2011), Graph analysis of epileptogenic networks in human partial epilepsy. Epilepsia 52:84-93.

Yan CG, Zang YF (2010), DPARSF: A MATLAB Toolbox for "Pipeline" Data Analysis of Resting-State fMRI. Frontiers in systems neuroscience 4:13.

Yarkoni T, Poldrack RA, Nichols TE, Van Essen DC, Wager TD (2011), Large-scale automated synthesis of human functional neuroimaging data. Nat Methods 8:665-670.